Journal of Nuclear Medicine, published on September 13, 2019 as doi:10.2967/jnumed.119.231167

A Clinical Feasibility Study To Image Angiogenesis in Patients With Arteriovenous Malformations Using ^{68}Ga-RGD PET/CT.

SHORT TITLE

RGD PET/CT in arteriovenous malformation

AUTHORS

Daphne Lobeek[1]; Frédérique C.M. Bouwman[1]; Erik H.J.G. Aarntzen[1]; Janneke D.M. Molkenboer-Kuenen[1]; Uta E. Flucke[2]; Ha-Long Nguyen[3]; Miikka Vikkula[3,4]; Laurence M. Boon[3,4]; Willemijn Klein[1,5]; Peter Laverman[1]; Wim J.G. Oyen[1,6,7]; Otto C. Boerman[1]; Samantha Y.A. Terry[8]; Leo J. SchultzeKool[1,5] Mark Rijpkema[1]

AFFILIATIONS

[1]Department of Radiology and Nuclear Medicine, Radboud University Medical Center Nijmegen, Nijmegen, The Netherlands

[2]Department of Pathology, Radboud University Medical Center Nijmegen, Nijmegen, The Netherlands

[3]Human Molecular Genetics, de Duve Institute, University of Louvain, Brussels, Belgium

[4]Center for Vascular Anomalies (VASCERN VASCA European Reference Center), Division of Plastic Surgery, Cliniques Universitaires Saint-Luc, Brussels, Belgium

[5]Center for Vascular Anomalies (VASCERN VASCA Reference Center), Department of Radiology and Nuclear Medicine, Radboud University Medical Center Nijmegen, Nijmegen, The Netherlands

[6]Department of Biomedical Sciences, Humanitas University, Milan, Italy

[7]Department of Radiology and Nuclear Medicine, Rijnstate Hospital, Arnhem, The Netherlands

[8]Department of Imaging Chemistry and Biology, School of Biomedical Engineering & Imaging Sciences, King's College London, King's Health Partners, St Thomas' Hospital, London, United Kingdom

Correspondence to: D. Lobeek (daphne.lobeek@radboudumc.nl), Department of Radiology and Nuclear Medicine, Radboud University Medical Center, P.O. Box 9101, 6500HB, Nijmegen, Netherlands, telephone number: +31(0)243614510, fax number: +31(0)243618942.

Word counts: 4995

ABSTRACT

Objective: Arteriovenous Malformations (AVMs) have an inherent capacity to form new blood vessels resulting in excessive lesion growth and this is further triggered by the release of angiogenic factors. Gallium-68 (^{68}Ga) labeled arginine-glycine-aspartate tripeptide sequence (RGD) positron emission tomography (PET)/computed tomography (CT) imaging (^{68}Ga-RGD PET/CT) may provide insight in the angiogenic status and treatment response of AVMs. This clinical feasibility study demonstrates that ^{68}Ga-RGD PET/CT imaging can be used to quantitatively assess angiogenesis in peripheral AVMs.

Methods: Ten patients with a peripheral AVM (mean age 40 years, four men, six women) and scheduled for endovascular embolization treatment, were prospectively included. All patients underwent ^{68}Ga-RGD PET/CT imaging 60 min after injection (mean dose 207±5 MBq). Radiotracer uptake in AVM, blood-pool, and muscle activity were quantified as Standardized Uptake Values (SUV_{max}, SUV_{peak}) and descriptive analysis of the PET/CT images was performed. Furthermore, immunohistochemical analysis was performed on surgical biopsy material of peripheral AVMs to investigate the expression pattern of integrin $\alpha_v\beta_3$.

Results: ^{68}Ga-RGD PET/CT imaging showed enhanced radiotracer uptake in all AVM lesions (mean SUV_{max} 3.0±1.1; mean SUV_{peak} 2.2±0.9). Lesion/blood and lesion/muscle ratios were 3.5±2.2 and 4.6±2.8, respectively. Radiotracer uptake in AVMs was significantly higher compared to uptake in background tissue (p=0.0006 and p=0.0014) for blood and muscle, respectively. Initial observations include identification of radiotracer uptake in (multifocal) AVM lesions and enhanced radiotracer uptake in intra-osseous components in those AVM cases affecting the bone integrity. Immunohistochemical analysis revealed cytoplasmatic and cell membranous integrin $\alpha_v\beta_3$ expression in endothelial cells of AVMs.

Conclusion: This feasibility study showed increased radiotracer uptake in AVM with angiogenic activity compared to surrounding tissue without angiogenic activity, suggesting that ^{68}Ga-RGD PET/CT imaging

can be used as a tool to quantitatively determine angiogenesis in AVM. Further studies will be conducted to explore the potential of ^{68}Ga-RGD PET/CT imaging for guiding current treatment decisions and for assessment of response to anti-angiogenic treatment.

KEY WORDS

Arteriovenous malformation; PET/CT; RGD; integrin $\alpha_v\beta_3$; angiogenesis

INTRODUCTION

Arteriovenous Malformations (AVMs) are tangles of shunting blood vessels (nidus), in which the arteries are directly connected to a venous drainage network (*1*). AVMs are highly complex structures, in which angiogenic stimuli act in dynamic interplay with local hemodynamic conditions (*2,3*). Patients commonly present with deformations, abnormal pulsating masses, pain, hemorrhage, or ulcers at ages ranging from young-to-middle age (*4*). When left untreated, loss of organ function, cardiac overload, skin necrosis, and/or bleeding are serious complications. AVMs can manifest throughout the body, but in particular for those patients with AVMs located in the face or extremities, the effect on quality of life of having respectively a severe cosmetic defect or reduced mobility can be devastating.

Current treatment options of these congenital anomalies are still limited to either surgically remove the nidus or to occlude the nidus with endovascular embolization techniques. Unfortunately, both treatments have drawbacks and may show only partial response and/or severe damage to surrounding tissues (*5,6*). Furthermore, these interventions may cause hemodynamic changes to the AVM – initiating progression of disease at adjacent sites – resulting in increased complication risks, destabilization of the AVM, and a subsequent need for repeated interventions (*6*).

Recent advances in the understanding of AVM-related angiogenesis has stimulated the discussion on the use of systemic drugs targeting angiogenesis (*7,8*). However, effective application of anti-angiogenic drugs to patients is hampered by the lack of accessible tools to assess the presence and dynamics of angiogenesis within the AVM during the course of the disease. Therefore, molecular imaging techniques enabling visualization of angiogenesis are warranted to provide clinicians with quantitative outcome measures that can be used to monitor follow-up of treatment efficacy or to predict response to (anti-angiogenic) therapy.

Integrin $\alpha_v\beta_3$, expressed on activated endothelial cells of newly formed blood vessels, are an attractive target for radiopharmaceuticals allowing quantitative molecular imaging of angiogenesis using radiolabeled arginine-glycine-aspartate tripeptide sequence (or RGD) derivatives and PET/CT (*9,10*). Gallium-68 labeled dimeric RGD (or ^{68}Ga-RGD) is a radiopharmaceutical that binds integrin $\alpha_v\beta_3$ with high affinity and has shown its potential in tumor imaging (*11-14*). As the development of AVMs is closely related to angiogenesis, ^{68}Ga-RGD PET/CT imaging may enable quantitative assessment of angiogenesis in peripheral AVMs. The aim of this study was to assess the integrin $\alpha_v\beta_3$ expression levels in peripheral AVM and to determine the feasibility of ^{68}Ga-RGD PET/CT imaging to visualize angiogenesis in peripheral AVMs.

MATERIALS AND METHODS

Study Population

This prospective proof-of-concept study was approved by the regional Ethics Review Board. The study (EudraCT 2015-005809-36) is registered in Dutch trial register, no. NL56104.091.16. Written informed consent was obtained from all individual participants included in this study. All procedures performed in this study were in accordance with the ethical standards of the institutional and national research committee and with the 1964 Helsinki declaration.

Patients diagnosed with at least one peripheral AVM confined to the subcutaneous and/or muscle tissue, with or without an intraosseous component, were included. AVMs were classified by their flow dynamics, clinical behavior, and angioarchitecture according to the Yakes Classification (*15*). Patients were eligible if pre-operative imaging of the lesion (four-dimensional computed tomography angiography (4D-CTA) and angiographic imaging) were available, and patients were scheduled for percutaneous or transarterial embolization treatments with ethanol. Patients with contra-indications for ^{68}Ga-RGD PET/CT imaging (pregnancy, breast-feeding, or severe claustrophobia), and/or an impaired renal- or liver function (creatinine clearance ≤60 ml/min, aspartate aminotransferase and alanine aminotransferase levels ≥3x upper limit of normal, and total bilirubin ≥2x upper limit of normal), were ineligible. When ^{68}Ga-RGD PET/CT imaging was performed in between two treatments, imaging was scheduled at least six weeks after the last treatment to minimize potential radiotracer uptake related to treatment associated-inflammation.

^{68}Ga-RGD PET/CT Acquisition

Patients were intravenously administered with 207±7 MBq, 42±8 μg ^{68}Ga-RGD (range 197-215 MBq and 34-58 μg respectively) using a slow bolus injection of 8 ml over 1 min. For radiotracer preparation see the description as provided in supplemental material 1. Patients had no restrictions in

food or medicine intake, and were asked to void before scanning. At 61±6 min post injection, ^{68}Ga-RGD PET/CT images were acquired using a Siemens Biograph 40 mCT scanner (Siemens Healthcare). A low-dose CT scan (512x512 voxels; 0.98x0.98x5 mm^3 voxel size; 1 pitch; 16x1.2 mm) was acquired for attenuation correction and anatomical reference, with an automatically modulated x-ray tube voltage and current (120 kV, 50 mA) using Care kV and Care Dose4D (Siemens Healthcare). The PET images were acquired in list-mode with 10 min per bed position, with the field of view covering the entire arteriovenous malformation (200x200 matrix size; 4.07x4.07x5 mm^3 voxel size; 2 to 3 bedpositions (225-725 mm field-of-view covering)). The CT images were reconstructed with a B31f convolution kernel. The PET images were reconstructed using a 3D ordered-subset expectation maximization algorithm with a spatially varying point-spread function incorporating time-of-flight information; 3 iterations and 21 subsets; a 200x200 matrix (2.04 mm pixel size). A three-dimensional Gaussian filter kernel with a full-width-at-half-maximum of 3.0 mm and transaxial matrix size of 200x200 mm was used as post reconstruction filter.

Safety analysis included the recording of adverse events according to Common Terminology Criteria for Adverse Events, version 4.03, recording of changes in vital signs (blood pressure, temperature, and heart rate) before and up to two hours after radiotracer injection, and included laboratory measurements, including hemocytology, kidney function (creatinine clearance, urea), and liver function (aspartate aminotransferase level, alanine aminotransferase level, total bilirubin), at baseline and one week after radiotracer injection. A study flowchart is provided in supplemental figure 1.

^{68}Ga-RGD PET/CT Image Analysis

Visual image analysis and AVM detection was performed using Oasis Software (version 1.9; Segami Corporation, Columbia, MD, USA). PET quantification was performed with Inveon Research Workspace software (version 2.04; Siemens, Erlangen, Germany). When patients showed multiple AVMs, only the AVM that was or would be embolized was delineated. For radiotracer uptake in muscle and

arterial tissue, a spherical volume of interest (VOI) with a 3 cm diameter was defined manually in CT images and subsequently transferred to the registered PET images. The segmentation of this VOI depended on the localization of the AVM and its surrounding tissue present within PET field of view. For the relationship to intensity of uptake in areas with physiological radiotracer uptake, spherical VOIs in liver, spleen, mediastinum, and kidney were drawn. The information within all VOIs was subsequently exported to MATLAB version R2014b (MathWorks, Natick, MA, USA) to calculate maximum and peak standardized uptake values (SUV_{max} and SUV_{peak}). SUV_{peak} was determined using in-house developed software by generating a mean SUV of the voxel with highest uptake (SUV_{max}) and its surrounding voxels representing a sphere of 1 cm^3. Lesion/blood- and lesion/muscle ratios were calculated as follows: $\frac{SUV_{peak,lesion}}{SUV_{peak,blood}}$ and $\frac{SUV_{peak,lesion}}{SUV_{peak,muscle}}$, respectively.

Immunohistochemical Analysis

5-µm sections of frozen (n=3) and paraffin-embedded (n=7) surgical biopsy material from the lip, orbita, cheek, finger, foot, lower leg, and back of peripheral AVMs was used for immunohistochemical analysis. Tissue samples were stained for integrin $\alpha_v\beta_3$ expression (anti-$\alpha_v\beta_3$ integrin monoclonal antibody, MAB1976B, clone LM609, 10 µg/ml, Merck Millipore (frozen sections) and AB7166, clone BV3, 1:100, Abcam (paraffin sections)), microvascular density (anti-CD31 monoclonal antibody, 1:50, ab28364, Abcam), and hematoxylin-and-eosin. Evaluation by light microscopy was performed in which staining patterns, including the evaluation of the endothelium of vessels and/or normal tissues, were assessed.

Statistical Analysis

Values are represented as mean ± standard deviation. Graphs were made and statistical analyses of SUV_{peak} values were performed using GraphPad Prism 5.03 (Graph Pad Software, Inc, La Jolla, CA). Differences in background tissue uptake were tested for significance using a one-way ANOVA test with post hoc Bonferroni adjustments. Statistically significant differences between radiotracer uptake and

background was tested using a paired sample t-test. An α-value of 0.05 was used in all analyses. Pattern of staining were scored semi-quantitatively according to staining intensity and extension in the whole slide (0: no staining; 1: weak staining; 2: moderate staining; 3: strong staining).

RESULTS

Patient Population

Six women and four men (mean age 43 y ± 17 and 34 y ± 8, respectively) participated in this pilot study. Patient characteristics are given in Table 1. One patient (#7) underwent ^{68}Ga-RGD PET/CT imaging before first endovascular embolization therapy, four patients (#1, #2, #5, and #10) underwent ^{68}Ga-RGD PET/CT imaging on average 2.5 months (range 2-3 months) after last treatment, three patients (#3, #8, and #9) were scheduled for a new treatment after nine months, due to underlying complications. One patient (#4) underwent ^{68}Ga-RGD PET/CT imaging six months after the last intervention, but during the next intervention no nidus was found and therefore embolization could not be performed. One patient (#6) showed slowly progressive disease (increased pain) and underwent ^{68}Ga-RGD PET/CT imaging before first embolization therapy after eight years.

^{68}Ga-RGD PET/CT Imaging Of AVM

There were no adverse or clinically detectable injection-related (serious) adverse events nor any changes in vital signs in any of the subjects. No significant changes in vital signs were observed, and blood analysis before and one week after ^{68}Ga-RGD tracer injection showed laboratory values within normal ranges, no clinically relevant changes were observed (data not shown).

All lesions, as defined on conventional angiographic images, could be readily identified on ^{68}Ga-RGD PET/CT scans independently of the location or size of the AVM, with lesion/blood and lesion/muscle ratios of 3.5±2.2 and 4.6±2.8, respectively. In all patients radiotracer accumulation corresponded to the location of the nidus as defined by plain angiographic and 4D-CTA images (figure 1). Mean SUV_{max} and SUV_{peak} of radiotracer uptake were 3.0 (range 1.0-4.6) and 2.2 (range 0.7-3.6) respectively. Uptake within the lesion was significantly higher than radioactivity levels in blood (p=0.0014) and muscle (p=0.0006). The uptake of ^{68}Ga-RGD as defined with SUV_{peak} measurements in all AVMs and normal tissues are shown

in figure 2. Radiotracer uptake in blood-pool and muscle was comparable in all patients even with variances in blood-pool and muscle selection. The mean radiotracer uptake between blood-pool and muscle was not statistically significant different (p=0.11). An example of the range of physiological radiotracer uptake in different organs is provided in supplemental figure 2.

In nine out of ten patients, the hotspots in the ^{68}Ga-RGD PET/CT images co-localized with the center of the AVM as revealed on 4D-CTA and angiographic images. Interestingly, ^{68}Ga-RGD PET/CT images revealed a PET-positive lesion within the palmar side of the right hand of patient #9, whereas angiographic imaging did show a diffuse and complex AVM with multiple enlarged feeding arteries and an increased venous drainage pattern.

In contrast to the low variance in background tissue between the patients, a considerable variance in radiotracer uptake between patients within the AVM was observed (figure 2). Because all study subjects underwent ^{68}Ga-RGD PET/CT imaging either before the first treatment or in between two treatments, an exploratory analysis of the correlation between therapy status and ^{68}Ga-RGD uptake values was performed (supplemental figure 3).

^{68}Ga-RGD Uptake In Symptomatic And Asymptomatic Lesions

According to the presence of patients' pain symptoms at the location of the AVM nidus (symptomatic lesions), ^{68}Ga-RGD PET/CT images revealed enhanced radiotracer uptake in the tissues adjacent to the nidus in five patients (patient #3, #6, #7, #8, and #10), suggesting uptake in asymptomatic lesions as well. In two patients (patient #6 and #8), this increased uptake corresponded to an additional nidus also observed on conventional imaging. However, in the other patients, these findings may indicate upregulated integrin $\alpha_v\beta_3$ expression through endothelial cell activation adjacent to the treated nidus, which could not be assessed by conventional imaging (white arrow in figure 3A and supplemental figure 4). High radiotracer uptake was also observed within the intra-osseous component

of three AVMs (patient #3, #7, and #10), as indicated with the yellow arrow in figure 3B. Patient #3 previously suffered from an extensive symptomatic AVM in the distal part of the foot, which was treated with multiple embolization therapies. The ^{68}Ga-RGD PET/CT images showed significantly lower radiotracer uptake in the distal part of the foot as compared to the active nidus in the more proximal part, and a few persistent foci with enhanced activity around the toes (figure 1C), indicating reduced angiogenic activity after treatment.

Immunohistochemical Analysis

Integrin $\alpha_v\beta_3$ expression could be confirmed by immunohistochemical analysis of surgical AVM tissue. Cytoplasmatic and cell membranous integrin $\alpha_v\beta_3$ expression in endothelial cells of AVMs was observed, showing positive staining both for some arterial (scale 0-2) and venous endothelial cells (2) as correlated with endothelial cell staining with CD31. In addition, in some tissue samples, expression of integrin $\alpha_v\beta_3$ was observed on erythrocytes (0-2) and smooth muscle cells mainly of the vessel walls (scale 0-1). However, this staining was weak and background staining could not be excluded. A typical example of the immunostaining is given in figure 4.

DISCUSSION

This proof-of-concept study showed the feasibility of ^{68}Ga-RGD PET/CT imaging in peripheral AVMs. We demonstrated that ^{68}Ga-RGD uptake is increased in the nidus in patients with AVMs and that this uptake can be readily detected with good contrast between lesion and background tissue. This allowed delineation of regions with and without enhanced integrin $\alpha_v\beta_3$ expression within an AVM.

Although the integrin $\alpha_v\beta_3$ expression pattern and its role in tumors, wound healing, and chronic inflammation has already been shown (*16-18*), data on integrin $\alpha_v\beta_3$ expression and its role in AVM have been limited to cerebral vascular malformations (*19*). The angiogenic process in AVM is upregulated by pathologic and physiologic conditions, such as traumas, endothelial shear stress, and immune- or inflammatory stimuli (*20,21*). These conditions induce the expression of vascular endothelial growth factors (VEGF), cytokines (IL-6, TNF-α), and other endogenous modulators (such as HIF-1α), thereby enhancing migration and proliferation of endothelial and smooth-muscle cells, resulting in the formation of new blood vessels (*21*). Immunohistochemical analysis showed endothelial cell expression of $\alpha_v\beta_3$ integrins, however, a more extensive histological assessment is required to examine potential contributions of extracellular matrix remodeling through activated macrophages, which have been shown to also express $\alpha_v\beta_3$ integrins (*22*). The integrin $\alpha_v\beta_3$ expression pattern on smooth muscle cells and erythrocytes are in line with previous publications (*23*).

In patients with intra-osseous involvement, integrin $\alpha_v\beta_3$ was upregulated in those parts of the AVM that showed bone deformation. It is likely that this observed radiotracer uptake pattern in these patients is due to binding of ^{68}Ga-RGD to integrin $\alpha_v\beta_3$ expressed both on osteoclasts and endothelial cells, because activated osteoclasts express high amounts of integrin $\alpha_v\beta_3$ to regulate cell-matrix interactions and intracellular signals responsible for bone resorption (*24*). This finding may have

consequences for treatment approaches, especially in those patients that need clinical follow-up to prevent pathological fractures.

Although the number of patients included was relatively small, we have made some interesting observations as potential future applications of the use of ^{68}Ga-RGD PET/CT in peripheral AVMs. ^{68}Ga-RGD PET/CT identified additional foci of integrin $\alpha_v\beta_3$ expression in two patients as compared to conventional angiographic imaging and revealed a clear nidus in a complex AVM that was not revealed on conventional imaging. These ^{68}Ga-RGD PET/CT findings may possibly have implications for treatment planning in those patients without a clear nidus visible on angiography, or in patients with a complex and/or large size AVM. Previous studies demonstrated that the lack of standardized and accurate interpretation of images from conventional imaging techniques in complex AVMs hamper correct diagnosis and accurate treatment planning (*25*). Furthermore, 4D-CTA and plain angiographic imaging provide detailed information on the extent and angioarchitecture of the AVM, but it will need further investigation whether ^{68}Ga-RGD PET/CT could be used to evaluate the angiogenic status of AVMs that should be considered as therapeutic target.

There are some limitations of the current feasibility study. Whereas ^{68}Ga-labeled RGD derivatives showed favorable radiochemistry, radiolabeling properties, and tumour-to-normal tissue ratios (*12*), the image resolution of ^{68}Ga-labeled radiotracers is in general inferior to ^{18}F-labeled radiotracers (*26*). Furthermore, the contribution from non-specific uptake to ^{68}Ga-RGD accumulation cannot be excluded, but as RGD radiotracers have shown a rapid clearance from the circulation, the enhanced permeability and retention effect is unlikely to play a major role in these lesions. Another limitation is that only one time point per patient was acquired. Therefore, an appropriate statistical analysis of the changes in angiogenesis pre- and post embolization was not feasible. Longitudinal ^{68}Ga-RGD PET/CT scans within the same patient – acquired in combination with conventional imaging, at

baseline and during the course of embolization treatment – would be needed to investigate whether ^{68}Ga-RGD PET/CT could predict response to therapy.

A few case reports have reported a role for novel anti-angiogenic therapeutics in the treatment of peripheral AVM (*27-29*). The expression of integrin $\alpha_v\beta_3$ in peripheral AVMs paves the way to further evaluate anti-angiogenic treatments for AVMs and the role of ^{68}Ga-RGD PET/CT imaging in the development of these anti-angiogenic therapies. Besides, ^{68}Ga-RGD PET/CT imaging may have the potential to provide quantitative information on the underlying pathogenesis of AVMs. New prospective clinical trials are warranted to determine how this novel imaging technique can improve our understanding of angiogenesis in AVM, and furthermore, how ^{68}Ga-RGD PET/CT can be used to investigate its potential to personalize treatment of AVM patients.

CONCLUSION

In this study, we demonstrated the feasibility of ^{68}Ga-RGD PET/CT imaging to visualize integrin $\alpha_v\beta_3$ expression in peripheral AVM. It may provide important complementary information to conventional angiographic imaging and could potentially be a valuable tool for the assessment of angiogenesis. These findings stimulate further studies on the exact role of angiogenesis in AVM which are needed to study the potential role of ^{68}Ga-RGD PET/CT imaging in the management of AVMs and/or guidance of treatments with novel drugs targeting angiogenesis.

DISCLOSURES

D.L. is supported by a grant obtained from The Netherlands Organisation for Health Research and Development (ZonMW), no. 95104005. H-L.N. received a Pierre M fellowship. S.Y.A.T. is supported by the Wellcome/EPSRC Centre for Medical Engineering [WT 203148/Z/16/Z] and King's College London and UCL Comprehensive Cancer Imaging Centre and funded by the CRUK and EPSRC in association with the MRC and DoH (England). L.B. is in part supported by the Fonds de la Recherche Scientifique – FNRS grant T.0146.16. M.V., L.B., W.K., and L.J.S.K. are members of the Vascular Anomalies Working Group of the European Reference Network (VASCERN) - Project ID 769036. No other potential conflicts of interest relevant to this article exist.

ACKNOWLEDGEMENTS

The authors thank the colleagues of the Radiopharmacy of the Departments of Radiology & Nuclear Medicine and Pharmacy for assistance during preparation of the radiopharmaceuticals. We furthermore thank W-J. van der Woude, P.J.M. Kok, M. de Groot, J.J.F. Thijssen, M. Boss, and V.C.J. van de Crommert for their assistance during screening of the patients and/or work-up of the ^{68}Ga-RGD PET/CT scans, and R.W. Ten Broek and L. Libbrecht for their assistance with the immunohistology.

KEY POINTS

Question: Can ^{68}Ga-RGD PET/CT imaging be used to visualize angiogenesis in peripheral arteriovenous malformations?

Pertinent findings: This proof-of-concept study showed that ^{68}Ga-RGD PET/CT enables the visualization of $\alpha_v\beta_3$ integrins in peripheral arteriovenous malformations. Tracer uptake in arteriovenous malformations was significantly higher compared to uptake in background tissue, with lesion/blood and lesion/muscle ratios of 3.5 ± 2.2 and 4.6 ± 2.8, respectively.

Implications for patient care: Future studies may reveal whether ^{68}Ga-RGD PET/CT may act as a complementary molecular imaging technique to the existing imaging modalities and may guide the application of novel anti-angiogenic drugs in peripheral AVMs.

REFERENCES

1. Cordisco MR. *Part IIId. Arteriovenous Malformations - Vascular Anomalies in Childhood*: Colegio Iberolatinoamericano de Dermatologia (CILAD); 2016:p244-356.

2. Lu L, Bischoff J, Mulliken JB, Bielenberg DR, Fishman SJ, Greene AK. Increased endothelial progenitor cells and vasculogenic factors in higher-staged arteriovenous malformations. *Plast Reconstr Surg.* 2011;128:260e-269e.

3. Rangel-Castilla L, Russin JJ, Martinez-Del-Campo E, Soriano-Baron H, Spetzler RF, Nakaji P. Molecular and cellular biology of cerebral arteriovenous malformations: a review of current concepts and future trends in treatment. *Neurosurg Focus.* 2014;37:E1.

4. Ogilvy CS, Stieg PE, Awad I, et al. Recommendations for the management of intracranial arteriovenous malformations: a statement for healthcare professionals from a special writing group of the Stroke Council, American Stroke Association. *Circulation.* 2001;103:2644-2657.

5. Lee BB, Baumgartner I, Berlien HP, et al. Consensus Document of the International Union of Angiology (IUA)-2013. Current concept on the management of arterio-venous management. *Int Angiol.* 2013;32:9-36.

6. Do YS, Yakes WF, Shin SW, et al. Ethanol embolization of arteriovenous malformations: interim results. *Radiology.* 2005;235:674-682.

7. Walker EJ, Su H, Shen F, et al. Bevacizumab attenuates VEGF-induced angiogenesis and vascular malformations in the adult mouse brain. *Stroke.* 2012;43:1925-1930.

8. Colletti G, Dalmonte P, Moneghini L, Ferrari D, Allevi F. Adjuvant role of anti-angiogenic drugs in the management of head and neck arteriovenous malformations. *Med Hypotheses.* 2015;85:298-302.

9. Haubner R, Maschauer S, Prante O. PET radiopharmaceuticals for imaging integrin expression: tracers in clinical studies and recent developments. *Biomed Res Int.* 2014;2014:871609.

10. Hong H, Chen F, Zhang Y, Cai W. New radiotracers for imaging of vascular targets in angiogenesis-related diseases. *Adv Drug Deliv Rev.* 2014;76:2-20.

11. Lobeek D, Franssen GM, Ma MT, et al. In vivo characterization of four (68)Ga-labeled multimeric RGD peptides to image alphavbeta3 integrin expression in two human tumor xenograft mouse models. *J Nucl Med.* 2018.

12. Dijkgraaf I, Yim CB, Franssen GM, et al. PET imaging of alphavbeta(3) integrin expression in tumours with (6)(8)Ga-labelled mono-, di- and tetrameric RGD peptides. *Eur J Nucl Med Mol Imaging.* 2011;38:128-137.

13. Arrieta O, Garcia-Perez FO, Michel-Tello D, et al. Response Assessment of (68)Ga-DOTA-E-[c(RGDfK)](2) PET/CT in Lung Adenocarcinoma Patients Treated with Nintedanib Plus Docetaxel. *J Nucl Med.* 2018;59:403-409.

14. Terry SY, Abiraj K, Frielink C, et al. Imaging integrin alphavbeta3 on blood vessels with 111In-RGD2 in head and neck tumor xenografts. *J Nucl Med.* 2014;55:281-286.

15. Yakes W.F. VRL, Ivancev K., Yakes A.M. . New Arteriographic Classification of AVM Based on the Yakes Classification System. In: Kim YW. LB, Yakes W., Do YS., ed. *Congenital Vascular Malformations*. Berlin, Heidelberg: Springer; 2017.

16. Desgrosellier JS, Cheresh DA. Integrins in cancer: biological implications and therapeutic opportunities. *Nature Reviews Cancer.* 2010;10:9-22.

17. Schnittert J, Bansal R, Storm G, Prakash J. Integrins in wound healing, fibrosis and tumor stroma: High potential targets for therapeutics and drug delivery. *Adv Drug Deliv Rev.* 2018;129:37-53.

18. Avraamides CJ, Garmy-Susini B, Varner JA. Integrins in angiogenesis and lymphangiogenesis. *Nat Rev Cancer.* 2008;8:604-617.

19. Lim M, Haddix T, Harsh GR, Vogel H, Steinberg GK, Guccione S. Characterization of the integrin alpha v beta3 in arteriovenous malformations and cavernous malformations. *Cerebrovasc Dis.* 2005;20:23-27.

20. Buell TJ, Ding D, Starke RM, Webster Crowley R, Liu KC. Embolization-induced angiogenesis in cerebral arteriovenous malformations. *J Clin Neurosci.* 2014;21:1866-1871.

21. Mouchtouris N, Jabbour PM, Starke RM, et al. Biology of cerebral arteriovenous malformations with a focus on inflammation. *J Cereb Blood Flow Metab.* 2015;35:167-175.

22. Antonov AS, Antonova GN, Munn DH, et al. alphaVbeta3 integrin regulates macrophage inflammatory responses via PI3 kinase/Akt-dependent NF-kappaB activation. *J Cell Physiol.* 2011;226:469-476.

23. Max R, Gerritsen RR, Nooijen PT, et al. Immunohistochemical analysis of integrin alpha vbeta3 expression on tumor-associated vessels of human carcinomas. *Int J Cancer.* 1997;71:320-324.

24. Nakamura I, Duong LT, Rodan SB, Rodan GA. Involvement of alpha(v)beta3 integrins in osteoclast function. *J Bone Miner Metab.* 2007;25:337-344.

25. Madani H, Farrant J, Chhaya N, et al. Peripheral limb vascular malformations: an update of appropriate imaging and treatment options of a challenging condition. *Br J Radiol.* 2015;88:20140406.

26. Sanchez-Crespo A. Comparison of Gallium-68 and Fluorine-18 imaging characteristics in positron emission tomography. *Appl Radiat Isot.* 2013;76:55-62.

27. Bauditz J, Lochs H. Angiogenesis and vascular malformations: antiangiogenic drugs for treatment of gastrointestinal bleeding. *World J Gastroenterol.* 2007;13:5979-5984.

28. Pfohler C, Janssen E, Buecker A, Vogt T, Muller CS. Successful treatment of a congenital extra-truncal vascular malformation by orally administered propranolol. *J Dermatolog Treat.* 2015;26:59-62.

29. Burrows PE, Mulliken JB, Fishman SJ, Klement GL, Folkman J. Pharmacological treatment of a diffuse arteriovenous malformation of the upper extremity in a child. *J Craniofac Surg.* 2009;20 Suppl 1:597-602.

FIGURES

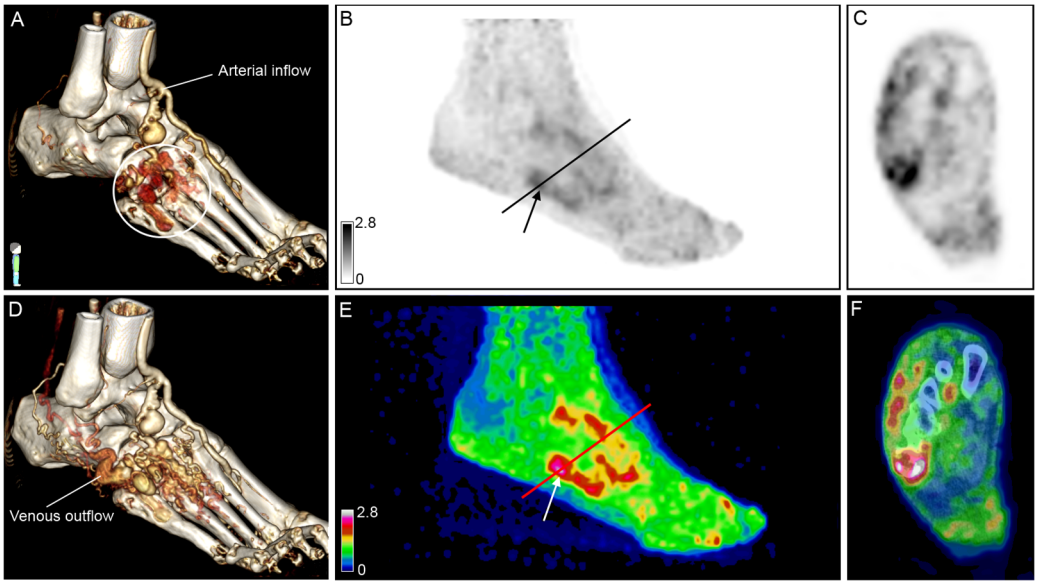

FIGURE 1: 3D reconstructions of 4D-CTA (A,B) and ^{68}Ga-RGD PET/CT (C) imaging of an arteriovenous malformation in the right foot of a male patient (44 y, #3). 3D reconstructions of 4D-CTA demonstrate an arterial input flow with the nidus indicated by the white circle (A) and venous outflow (D). Maximal intensity projection of ^{68}Ga-RGD PET image at 60 min after injection, showing radiotracer uptake within the lesion (SUV_{max} 3.0; SUV_{peak} 2.3), as indicated by the arrow (B, E). The black and red lines indicate axial view of the ^{68}Ga-RGD PET/CT images (C, F). This patient was previously treated with multiple embolizations for a symptomatic AVM in the distal part of the foot. The ^{68}Ga-RGD PET/CT images show significantly lower radiotracer uptake and a few persistent foci with enhanced activity around the toes (E). Arterial and venous flow of this part is not shown in A and D. Abbreviations: SUV, standardized uptake value.

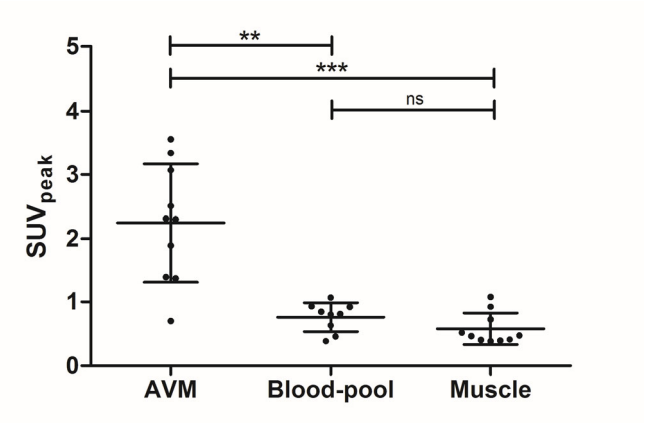

FIGURE 2: Scatter plot of peak standardized uptake values (SUV_{peak}) of arteriovenous malformation (AVM, mean 2.2 ± 0.9), blood-pool (mean 0.8 ± 0.2), and muscle activity (mean 0.6 ± 0.2) of each individual patient. Significance levels: ** $P < 0.005$; *** $P < 0.001$. ns = not significant.

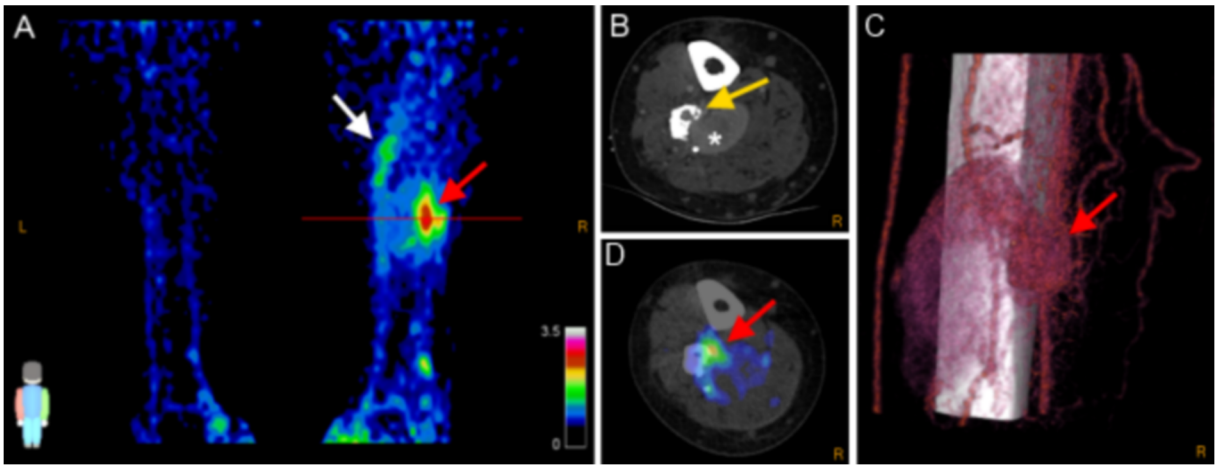

FIGURE 3: Maximal intensity projection of ^{68}Ga-RGD PET (A), CTA (B), fused axial ^{68}Ga-RGD PET/CT (C), and 3D reconstruction of 4D-CTA (D) of a male patient (38 y, #7) showing a nidus in right leg arteriovenous malformation (SUV_{max} 3.2; SUV_{peak} 2.5, red arrows). The red line in (A) corresponds to axial slides of (B) and (C). Both a heterogeneous uptake pattern of enhanced radiotracer uptake in tissue adjacent to the nidus at the more proximal part of the right leg (white arrow in (A)) and a bone deformation in fibula caused by compression and infiltration of vessels could be visualized (yellow arrow in (B)). Furthermore, a large venous aneurysm (asterisk in (B)) was present. The 3D reconstruction of 4D-CTA (D) showed the arterial flow with the nidus and fistula (red arrow), and upcoming venous flow with the large venous aneurysm. Abbreviations: SUV, standardized uptake value.

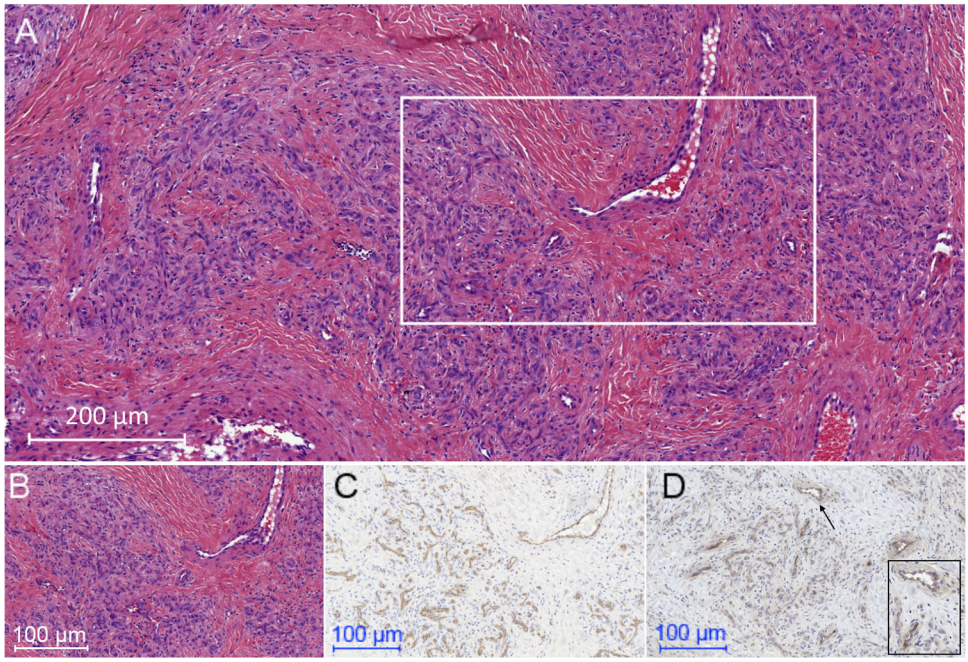

FIGURE 4: Typical example of the immunohistochemical analysis for the evaluation of $\alpha_v\beta_3$ integrin expression of an arteriovenous malformation. The highlighted region in (A) shows the detailed hematoxylin-and-eosin (B), anti-CD31 (C), and anti-$\alpha_v\beta_3$ integrin (D) staining (scalebar denotes 100 µm). CD31 staining demonstrated multiple small vessels within the field of view (C) and confirmed staining of $\alpha_v\beta_3$ integrin of these blood vessels (D). High-power magnification (50 µm) in (D) shows cell membranous $\alpha_v\beta_3$ integrin expression in endothelial cells of small blood vessels (black arrow, D).

TABLE 1: PATIENT CHARACTERISTICS.

Pt no. (#)	Age (y)	Gender	Yakes classification (*15*)	Location arteriovenous malformation
1	28	Male	IIIb	Chin
2	27	Male	II	Nose
3	44	Male	II	Right foot
4	51	Female	II	Finger, digit I right
5	64	Female	II	Finger, digit II right
6	57	Female	II	Finger, digit V left
7	38	Male	IIIa	Right lower leg
8	26	Female	II	Left upper leg
9	38	Female	II	Right hand
10	23	Female	II	Right elbow

SUPPLEMENTAL DATA

SUPPLEMENTAL MATERIAL 1.

ADDITIONAL INFORMATION ON PREPARATION OF RADIOTRACER

Preparation of the radiotracer ^{68}Ga-RGD$_2$

DOTA-E-[c(RGDfK)]$_2$ was synthesized by coupling E-[c(RGDfK)]$_2$ (Peptides International, Louisville, KY, USA) and DOTA(tris)Bu (1,4,7,10-Tetraazacyclododecane-1,4,7,10-tetraacetic acid) (Macrocyclics, Dallas, TX, USA), as described previously (*1-3*). Synthesis complied with Good Manufacturing Practice (GMP) regulations for human use.

Radiolabelling of DOTA-E-[c(RGDfK)]$_2$ was performed on a Scintomics GRP module (Scintomics GmbH, Fürstenfeldbruck, Germany) connected to one or two GMP-grade ^{68}Ge/^{68}Ga generators (IGG101 GalliaPharm, Eckert and Ziegler, Berlin, Germany). A Scintomics reagent and hardware kit for synthesis of ^{68}Ga-peptides using cationic purification (SC-01, ABX, Radeberg, Germany) was used for elution of the ^{68}Ge/^{68}Ga generator, radiolabelling, and purification of [^{68}Ga]Ga-DOTA-E-[c(RGDfK)]$_2$ (or ^{68}Ga-RGD$_2$). Briefly, ^{68}Ga was eluted from the ^{68}Ge/^{68}Ga generator with 0.1 N HCl and trapped on a PS-H$^+$ cartridge (Machery-Nagel GmbH, Düren, Germany). Subsequently, [^{68}Ga]GaCl$_3$ was eluted from the cartridge with 5 M NaCl into the reaction vial containing 70 µg DOTA-E-[c(RGDfK)]$_2$ in 1.5 M HEPES buffer, pH 7.0. After 15 min incubation at 100 ^{o}C, the mixture was loaded onto an activated SepPak C-18 Light cartridge (ABX, Radeberg Germany) for purification. The purified product was eluted with 50% ethanol in phosphate buffered saline (PBS), and subsequently filtered through a vented 0.22 µm filter unit into a closed sterile glass vial. Activity yield of ^{68}Ga-RGD$_2$ was 599 – 831 MBq (end of synthesis) and was measured in a dose calibrator (VDS-405, Comecer, Joure, The Netherlands).

After radiosynthesis, quality control of ^{68}Ga-RGD$_2$ was performed according to European Pharmacopoeia (Ph Eur) standards including verification of radiochemical purity and colloid content using reverse-phase high-performance liquid chromatography and instant thin-layer chromatography, pH

determination using a pH indicator strip, assessment of endotoxin content using Endosafe equipment (Charles River, Leiden, The Netherlands), and testing of sterility (coordinated by the Department of Pharmacy). All injected preparations met the quality control criteria and had a radiochemical purity >99%.

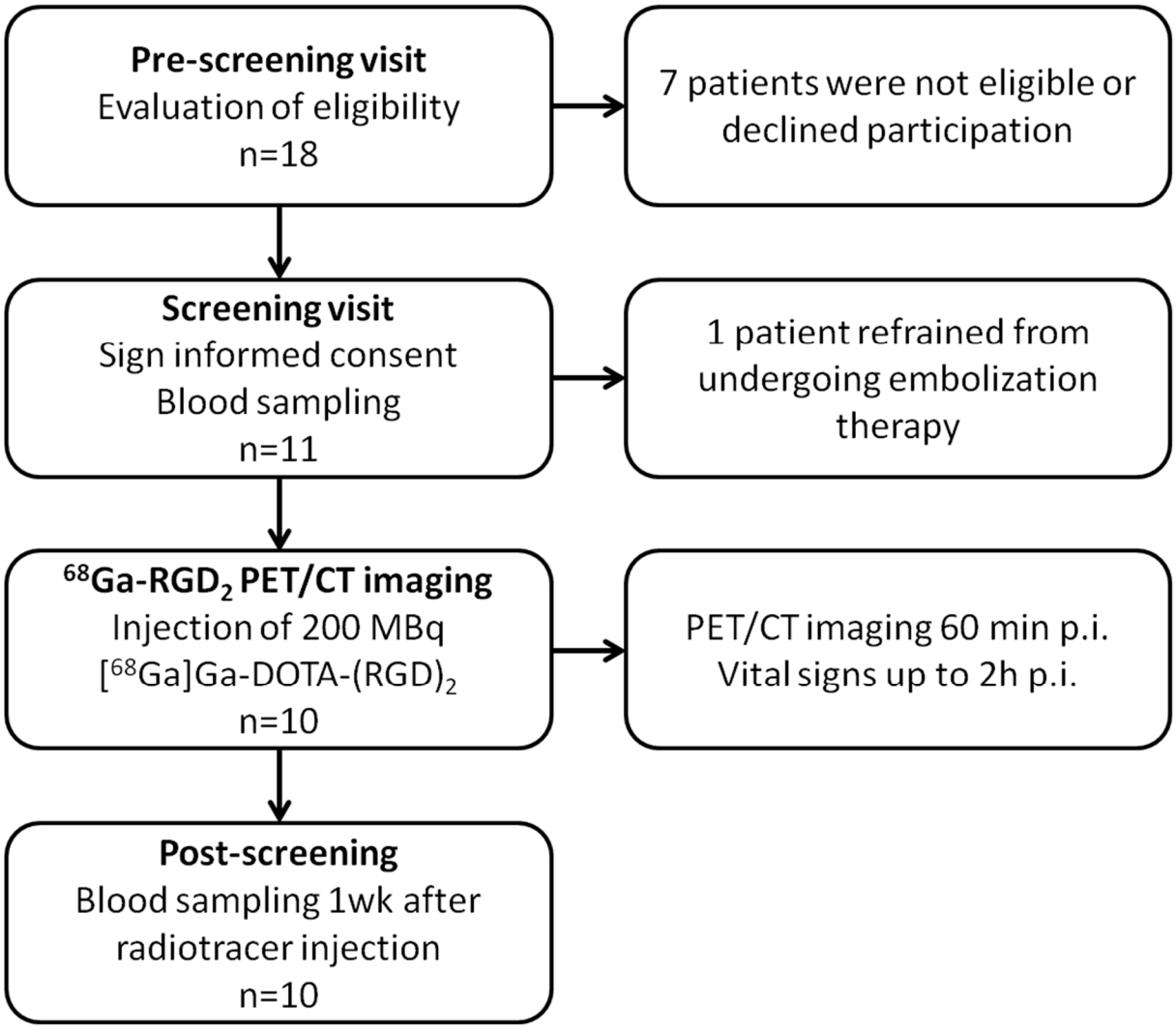

SUPPLEMENTAL FIGURE 1. Study flowchart of the study procedure using RGD-PET/CT imaging.

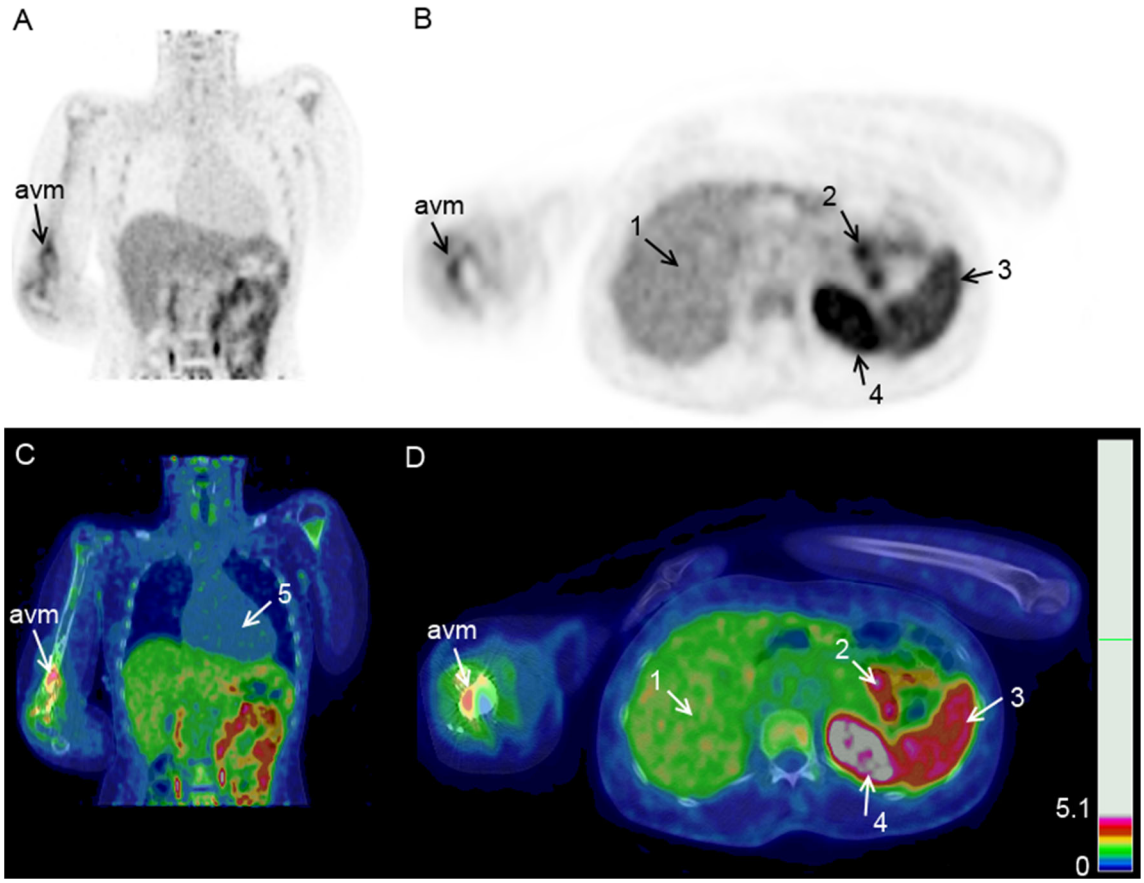

SUPPLEMENTAL FIGURE 2. A coronal and transversal ^{68}Ga-RGD PET slide (A and B), and coronal and transversal slide of a fused ^{68}Ga-RGD PET/CT scan (C and D) of a patient with an AVM in the upper right arm, illustrating the range of physiological radiotracer uptake in liver (1), small intestines (2), spleen (3), left kidney (4), and left ventricle blood pool (5), with an SUV_{max} and SUV_{peak} of 2.8 and 2.5 (liver), 17.2 and 12.9 (kidney), 4.3 and 2.0 (spleen), 1.2 and 1.0 (left ventricle blood pool), respectively.

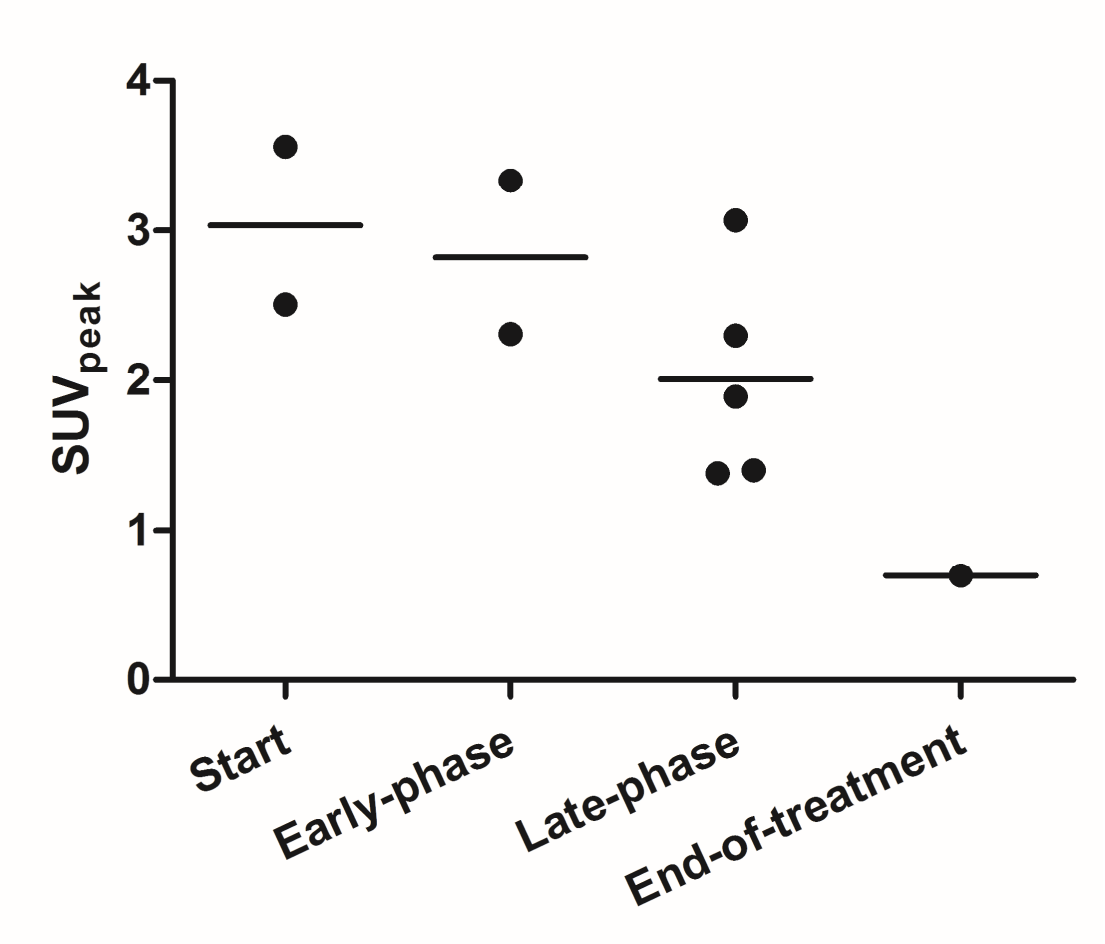

SUPPLEMENTAL FIGURE 3. Scatter plot of peak standardized uptake values (SUV_{peak}) of each individual patient with an arteriovenous malformation. Stage of treatment was defined as start (0; no treatment yet), early-phase (1; 1-3 embolizations, need for multiple embolizations), late-phase (2; 4-6 embolizations, need for embolization), or end-of-treatment (3; no new embolizations needed), at time of RGD-PET/CT imaging. Patients were put into categories based on stage of treatment, at time of RGD-PET/CT imaging), which suggest that higher radiotracer uptake levels are found in patients prior to and at early stages of treatment, whereas lower uptake values were observed in patients after multiple interventions or successful completion of treatment.